ORIGINAL RESEARCH PAPER

Low-altitude contour mapping of radiation fields using UAS swarm

Zachary Cook[1] · Monia Kazemeini[1] · Alexander Barzilov[1] · Woosoon Yim[1]

Abstract

This paper addresses the design of lightweight radiation sensors for the small-scale unmanned aerial system (UAS) and its implementation for low-altitude radiation source localization and contour mapping. The compact high-resolution gamma-ray CZT sensors were integrated into UAS platforms as plug-and-play components using robot operating system. The swarm of UAS has advantages over a single agent-based approach in detecting radiative sources and effectively mapping the area. The proposed swarm consists of three UAS platforms in a circular formation. The proposed approach can potentially be used for low-altitude clustered environments where a conventional helicopter-based platform cannot be utilized. It can provide a relatively precise boundary of the safe area for potential human exploration as well as enhancing situation awareness capabilities for first responders. The source seeking and contour mapping algorithms are developed based on a simple $1/R^2$ radiation field, but they are validated in more realistic radiation field having multiple sources and physical structures with scattering and attenuation effects simulated by MCNP code. Also, gradient estimation and contour mapping algorithms are validated experimentally with small-scale multicopter platforms in the indoor flight testbed.

1 Introduction

The deactivation and decommissioning process (D&D) includes the conversion of active, excess, and/or abandoned nuclear facilities to a final disposition [1, 2]. The use of UAS as aerial robotic platforms enables remote radiation sensing and sampling operations while keeping personnel out of the harm's way. D&D tasks require a suite of sensors, including radiation detectors that can be easily attached to UAS

✉ Woosoon Yim
woosoon.yim@unlv.edu

Zachary Cook
cookz2@unlv.nevada.edu

Monia Kazemeini
kazemei2@unlv.nevada.edu

Alexander Barzilov
alexander.barzilov@unlv.edu

[1] Department of Mechanical Engineering, University of Nevada, Las Vegas, 4505 S. Maryland Parkway, Las Vegas, NV 89154, USA

and utilized by first responders in field conditions. Recently, the cost of developing UAS platforms has dropped dramatically, and radiation sensing using multiple UAS has become economically viable, especially for low-altitude clustered environments.

Many researchers have studied UAS-based radiation detection and source seeking. A recursive Bayesian estimation approach was used in [3] for locating the source of a known model of radiation. This method uses a single UAS to measure the strength of a source via an onboard radiation sensor and uses an initial guess to predict the state and relative location of the source with respect to UAS. This method locates the source using current and previous measurements where the radiation sensor operates primarily as a distance sensor. A downside of this method can be its diversion from the actual state when measurements are noisy, or the source radiation is not modeled correctly. In this work, multiple UASs are used as a swarm for source seeking and contour mapping of radiation. Formation control has been studied extensively in many different applications in the past [4–14]. Most of this work is based on the circular formation of agents with an overall swarm heading angle determined by appropriate formation control schemes providing trajectories of each agent. A general mathematical framework of

multi-agent coordination based on a control Lyapunov function is studied in [8]. In [8], the proposed approached was applied and validated for two ground mobile robots carrying a beam. Arranz et al. [9] have done work related to the formation control of UAS swarm under limited communication range, which is applicable for most of the multicopter-based swarm control. This work is especially useful when agents perform collaborative tasks to navigate toward a priori unknown direction.

Different algorithms for determining the locations of radiation sources using simultaneous measurements taken from UAS swarm have been studied including the gradient-based method. Generally, to accomplish contour mapping, the swarm of UAS with onboard sensors uses gradient estimation to determine the steepest gradient direction which governs a bulk heading vector for the swarm to follow [10–12]. Moore et al. [10] studied source seeking by a circular formation of agents. In this work, the measurement of the signal is used to calculate an approximate gradient direction for steering the center position of multi-agent. Ogren et al. [15] have developed an algorithm for gradient detection where a networked group of UAS each with a single sensor adaptively determines the gradient. Source-seeking behavior can be accomplished by directing the swarm toward the most increasing gradient. Han et al. [12] show both the source seeking and contour mapping methods using a UAS. They first start with a source-seeking strategy then augment the heading direction of the swarm to move tangentially to the source once the reference contour is reached. However, conventional algorithms are effective only in a specific set of circumstances with particular initial conditions. Also, implementation of actual UAS in a swarm formation was not validated in an experimental testbed in the context of radiation source seeking and contour mapping. In [13], a formation control scheme is utilized for autonomous underwater vehicles (AUV) for ocean survey, monitoring, and search tasks. In this work, an adaptive path planning algorithm is studied for multiple AUVs based on Kalman filter-based model estimation using information collected by multiple AUVs. The similar formation control scheme has been applied to multiple autonomous ground vehicles (AGV). In [14], path planning parameter optimization algorithm is developed using an evolutionary strategy which saved a computational time and memory requirement significantly.

The presented circular formation algorithm is based on the gradient direction estimation by multi-agent studied in [8] and [10]. The main contribution of the current work is to adaptively change the circular swarm formation parameters to minimize the total flight paths of each UAS in source seeking and contour mapping tasks in the simulated radiation map created using MCNP (Monte Carlo N-Particle Transport Code). Also, the proposed algorithm is validated in the indoor flight testbed to check the feasibility

of real-time implementation in the field. The remainder of this paper is organized as follows. In Sect. 2, the onboard radiation sensor for the proposed swarm formation control is described. In Sect. 3, algorithms for source seeking and contour mapping are provided. Section 4 covers computer simulation platform used for validating the proposed algorithms, and selected experimental results are provided in Sect. 5.

2 Onboard radiation sensor

Radiation sensors are required for the use onboard of a UAS for high-resolution gamma-ray measurements in the field by the swarm of UAS. These sensors should be lightweight and of low power to enable their integration into the small-scale UAS platform that has a payload, battery power, and data processing limitations. Lightweight gamma radiation sensors have been studied previously including medium-resolution scintillator detectors and high-resolution ambient temperature detectors. However, UAS-ready sensor designs have not been extensively studied. The proposed radiation sensors are designed as compact, plug-and-play components which are vital for field operations: These sensors can be hot-plugged and hot-unplugged with the data acquisition and analysis fully automated. The onboard processing of gamma-ray spectra was utilized to reduce the data streams that require transmission significantly. The robot operating system (ROS) was utilized for data fusion by adding time and GPS parameters to the radiation data, thus enabling the UAS swarm control and cooperative sensing.

In this work, the Kromek CZT (cadmium zinc telluride) detector was used for its compact crystal size of 1 cm^3 and capability of high-resolution ambient temperature gamma-ray spectroscopy [15, 16]. The detector is USB-powered and suitable for mounting on a small-scale multicopter UAS used in this study. The CZT detector medium is a semiconductor that converts X-ray or gamma-ray photons into charge carriers. The detector module itself weighs only 49.2 g with dimensions of $2.5 \times 2.5 \times 6.1$ cm and uses a 1 cm^3 cadmium zinc telluride crystal. The sensor has an energy detection range from 30 KeV to 3.0 MeV with an energy resolution at 662 keV or less than 2%. The detector interfaces and is powered directly through a USB connector located on an onboard computer. Figure 1a, b shows the Kromek CZT detector and its mounted configuration on the UAS platform. The spectrum is generated from the counts obtained by the detector (as shown in Fig. 1c for 137Cs and 60Co sources). Mariscotti's technique [15] is used for identifying peaks and their intensities.

To integrate the radiation detector into the UAS, a plug-and-play design concept was used. This supports "hot plugging" of the detector into the UAS platform; thus, field
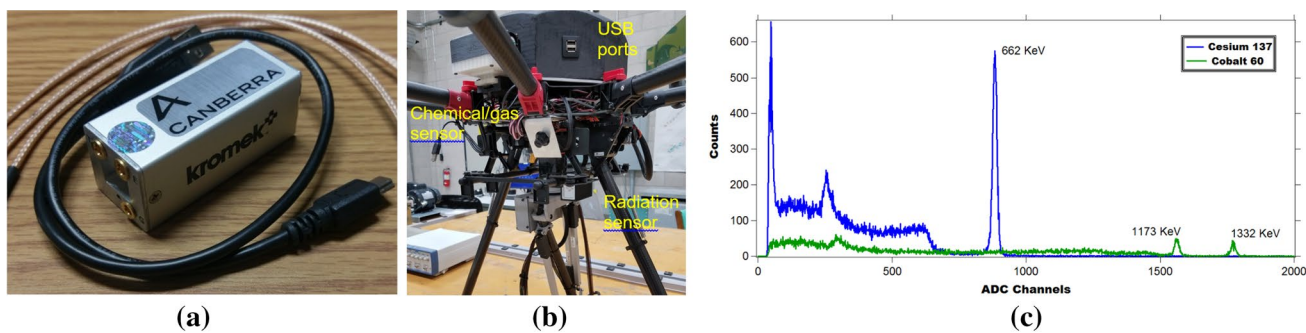
Fig. 1 **a** Kromek cadmium zinc telluride (CZT) detector; **b** CZT detector mounted on UAS; **c** Gamma-ray spectrum measured by the detector

operators do not need to set up component's parameters each time [17, 18]. Figure 2a shows the operational block diagram of this scheme. When a component is plugged, an operating system recognizes the component and installs a device driver to read and process sensor data as shown in Fig. 2b.

3 Algorithms for contour mapping

The swarm consists of three UASs, and circular formation is used in two-dimensional space. It is assumed that the radiation detector is mounted on each UAS for simultaneous radiation measurement. In this section, the contour mapping algorithm is presented along with gradient direction estimation and heading angle calculation schemes.

3.1 Gradient estimation

The contour mapping is based on two components: the gradient direction estimation and the average radiation level calculated using the radiation measurement data from sensors mounted on the UAS platforms of the swarm. The average of a scalar field is estimated over a circular area of radius r centered at a point c as shown in Fig. 6. T_{avg} is the average radiation level calculated using the data from sensors of three UASs flying in a circular formation.

$$T_{avg} = \frac{\int_{\Omega} T(x)\mathrm{d}x}{\pi r^2} \tag{1}$$

Here, Ω is the area of the circle, $T(x)$ is the intensity of the measured gamma peak of interest at a point x on the circle.
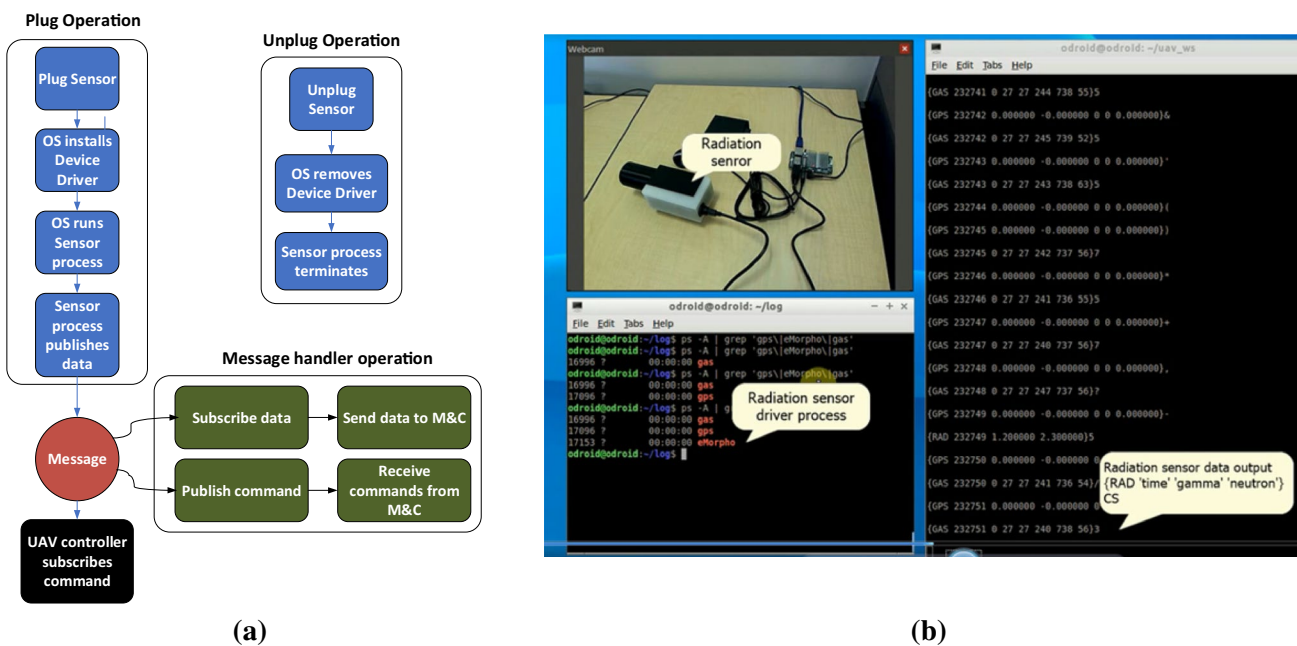

Fig. 2 **a** Operational block diagram of the plug-and-play operation. **b** Screenshots of plug-and-play operation of a radiation sensor

The formation center moves toward the increasing (a source-seeking method) or the constant (a contour mapping method) value of the average of sensor readings. To find the required direction of motion of the swarm's center, the gradient of T_{avg} should be determined using multiple readings T_n from the UAS's sensors. It is assumed that N measurements are taken out of the readings distributed inside the circle according to a known distribution (e.g., uniform or based on a $1/R^2$ model). Using the composite trapezoidal rule, the gradient is estimated [15] as

$$\nabla_c T_{avg} \approx \frac{2}{Nr^2} \sum_{i=1}^{N} T_n(p_i) p_i \Delta s \qquad (2)$$
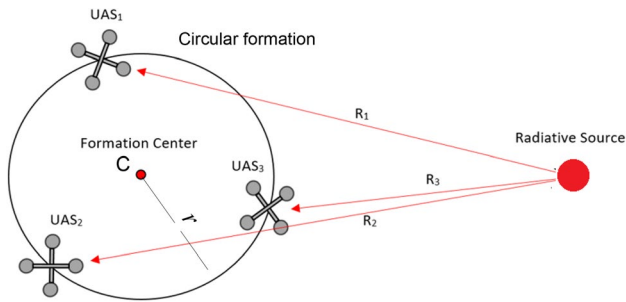
Fig. 3 A circular formation by three UASs with a radius of r. Radiation measurements $T(i)$ by three UAS ($i = 1, 2, 3$) based on $1/R^2$ model

where $p_i = x_i - c$ and $\Delta s = 2\pi r/N$. It should be noted that an origin of coordinate moved to the center of the circle, and the integral is approximated by a finite number of measurements N.

As shown in Fig. 3, three UASs in the swarm are distributed equally around a circle and $N = 3$ in (Eq. 2). Using (Eq. 2), horizontal and vertical components of the gradient can be determined. The formation center, c, can be moved relative to the current position using an estimated direction of the gradient for the source-seeking behavior for the swarm. Note that any number of UASs can be used for the swarm. With any number of UASs in the swarm, the gradient estimation requires each UAS to be evenly distributed around a circle for accurate estimation of the gradient. There is an inherent error in this gradient estimation algorithm within a $1/R^2$ field. A relatively small change in distance can have a significant effect on radiation measurement for each UAS depending on the relative orientation of the swarm to the source as well as its distance from the source. In the proposed contour mapping, three UASs will rotate about the swarm center c to improve gradient estimation by changing the relative direction of the source with respect to three UASs in action. Figure 4a shows how the gradient estimation error, ε, is defined in this study. It should be noted that the gradient estimation error increases when a source distance relative to a swarm center decreases as shown. In
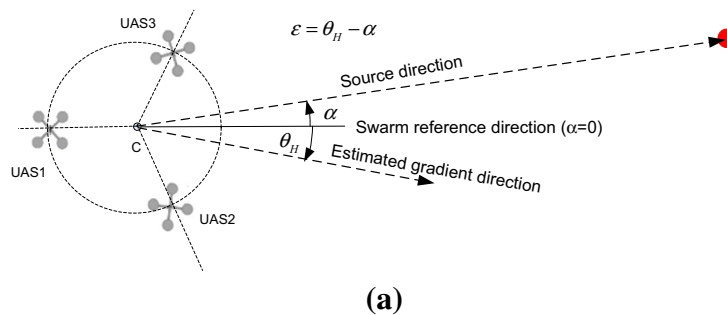
(a)
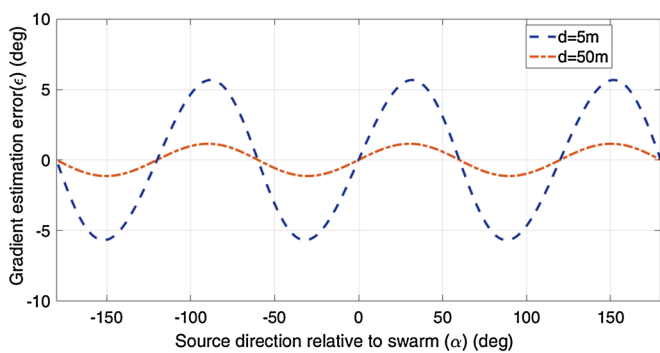
(b)
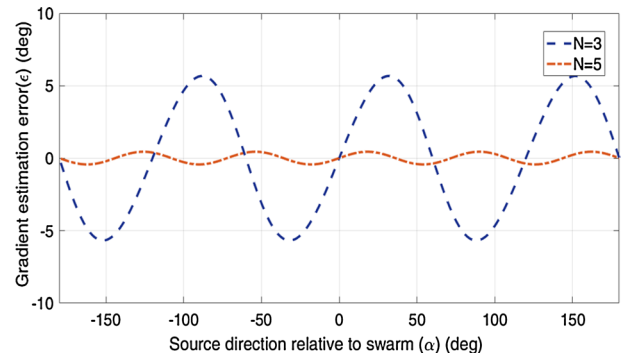
(c)

Fig. 4 Gradient estimation error from relative orientation between the source and UAS swarm for $N = 3$, swarm radius $= 1$ m, source distance $= 5$ m

other words, when the source is located far away from the swarm, the estimation error decreases as shown in Fig. 4b. As expected, the number of UASs in the swarm also affects the gradient error. Figure 4c shows error comparison which shows that more UAS in the swarm improves gradient estimation significantly. It should be noted that an adverse effect of gradient estimation near the target contour can be reduced by the spinning formation of swarm agents.

3.2 Heading angle

The bulkheading angle of the swarm ψ is determined by how far a UAS swarm is from the desired radiation contour to be mapped. As the swarm approaches the desired contour, the heading angle must be directed to a tangential direction of the contour. When the swarm is far away from the contour, the heading angle will be directed toward the source directly, which is a source-seeking behavior of the swarm as shown in Fig. 5.

As shown in Fig. 5, θ_H is an estimated steepest gradient direction and ϕ is a control angle determining a bulk heading angle ψ [19]. Note that all angles are measured with respect to a positive x-axis. The control angle ϕ is determined by how far the desired contour is located based on average radiation measurement $e_s = T_r - T_m$, where T_r is the desired radiation intensity of contour to be mapped and T_m is an average radiation intensity measurement by three UASs. Here, an arbitrary constant R is used along with R_c to calculate a heading angle of ψ. R_c is determined based on the PID control action from radiation measurement error or difference, e_s, with respect to the reference contour value T_m,

$$R_c = K_p e_s + K_d \frac{\mathrm{d}e_s}{\mathrm{d}t} + K_i \int e_s \mathrm{d}t,$$

$$\phi = \tan^{-1} \frac{R_c}{R}$$

$$(3)$$

where K_p, K_i, and K_d are proportional, integral, and derivative gains, respectively. It should be noted that the magnitude of R is arbitrary, and an arctangent in (Eq. 3) is used for mapping R_c to the control angle between 0° and 90°. As shown in (Eq. 3), a heading angle ψ becomes 90° for a large value of R_c, or the swarm is far away from the reference contour. For the swarm near the reference contour, R_c becomes small, and ψ becomes close to zero. This leads to the following equation for determining the heading angle ψ,

$$\psi = \theta_H - \frac{\pi}{2} + \phi \tag{4}$$

From (Eq. 4), it is evident that the swarm will move in a tangential direction near the reference contour and demonstrate a source-seeking behavior when it is far away from the source or reference contour.

4 Computer simulation

To validate the proposed contour mapping algorithms, two types of radiation fields were utilized. One is an ideal $1/R^2$ model for a radioactive source located at distance R from the sensor. This simplified model is used for properly tuning and improving contour mapping and source-seeking behaviors of the swarm. Improvements made for the proposed algorithm include the inclusion of UAS dynamics and adaptive spinning of the swarm for reduced flight trajectory of each UAS. The algorithm from the simplified radiation field is validated in more realistic radiation field containing physical obstacles and multiple sources computed with the MCNP code [20]. It should be noted that a stochastic nature of radiation sensing is considered for sensor data during simulation. Random noise was introduced to the radius value of the $1/R^2$ model. In the simulation, a noise on the order of 0 to ± 2.5 m is used which causes erratic gradient estimation and heading generation, as expected. To reduce this effect, a moving average filter is applied to both the gradient estimation and the heading angle generation. Figure 6 shows an overall simulation scheme used in the study.

4.1 UAS swarm simulation in a 1/R^2 field

As shown in Fig. 6b, the dynamics of UAS is incorporated for more realistic simulation of flight trajectories during
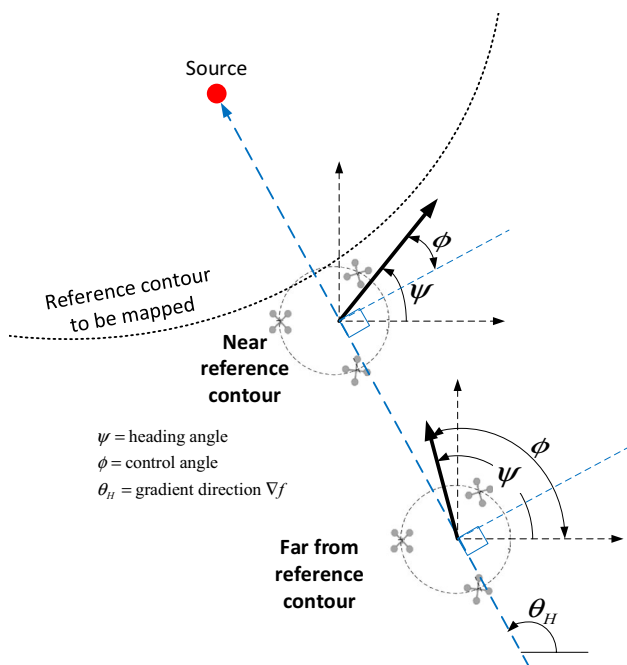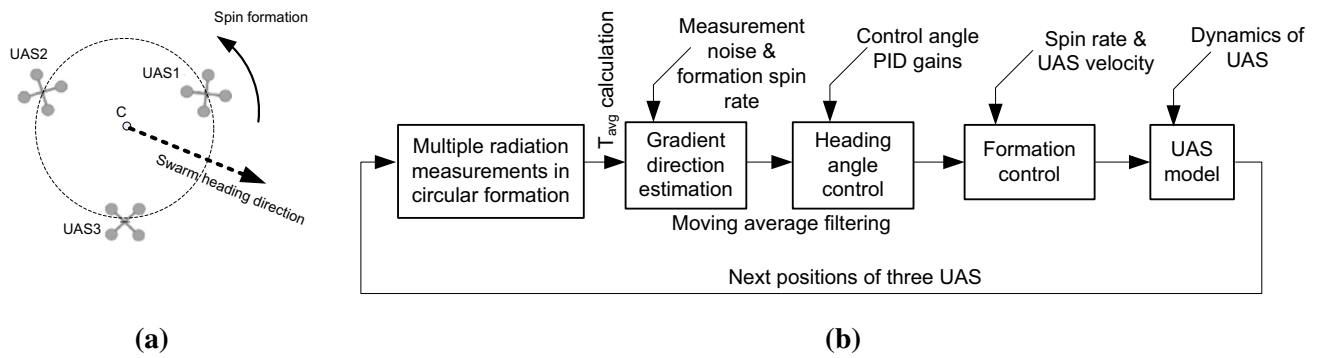

Fig. 5 A bulk heading angle of swarm Ψ and gradient angle θ_H

Fig. 6 **a** UAS spinning formation used to estimate the steepest gradient. **b** Overall simulation scheme used in the study

contour mapping and source seeking. In this simulation, instead of using just kinematic motions of each UAS, their dynamics was used to calculate their flight trajectories. Figure 7a shows the difference between inclusion and non-inclusion of UAS dynamics on their trajectories that the swarm can follow.

As mentioned previously, the spinning formation of the swarm improves estimation of radiation gradient direction [9, 19]. Spinning occurs around a virtual center of the formation, while the center of the formation moves with the desired vector to accomplish the contour mapping or source seeking. Figure 8 shows the effect of the spinning formation based on three UASs in the swarm. A bold line shows a path travelled by its formation center. As shown in 8b, non-spinning formation shows poor mapping performance primarily due to large gradient estimation errors which are

dependent on the relative direction of the source with respect to the swarm formation.

Having the swarm circling a virtual center while its center travels in the direction dictated by the swarm heading algorithm increases the total flight paths significantly. This leads to developing an adaptive spin rate adjustment scheme to avoid unnecessary spinning formation when it is not needed.

When the swarm is far away from the source or contour to be mapped, it is not necessary to spin the formation since their direction is nearly fixed. Once the swarm is near the contour, it is necessary to spin the formation since most contours have a curvilinear shape. The criterion for spinning is chosen as a radius of curvature of the formation center path. As shown in Fig. 9a, the swarm starts to spin its formation when it reaches near the contour to be followed. In this simulation, a spin rate control is saturated with a lower bound of
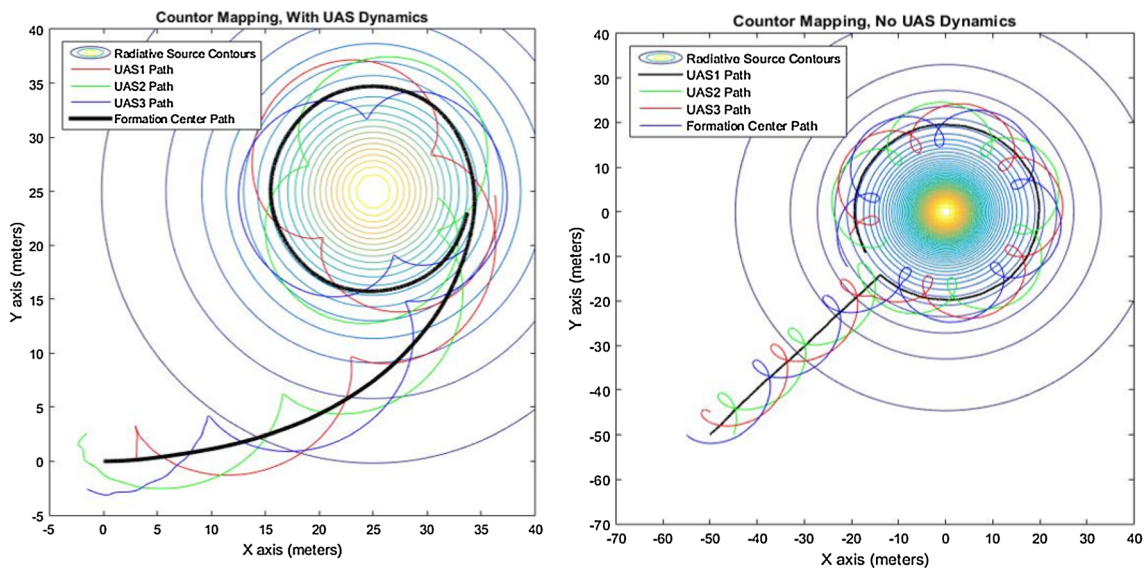
Fig. 7 A double integrator is incorporated in MATLAB to approximate UAS dynamics. This provides a more realistic simulation than when only kinematics is considered
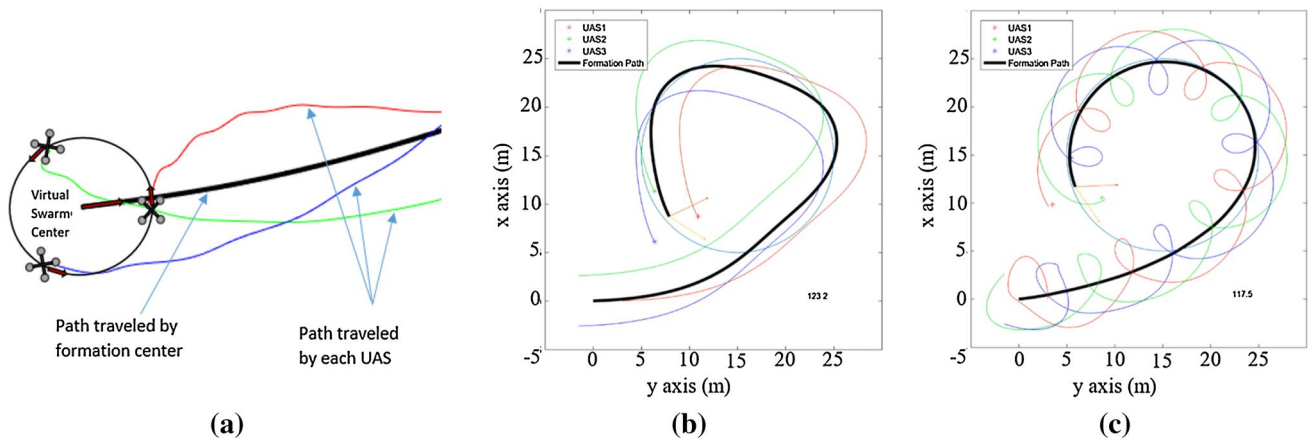
Fig. 8 **a** UAS swarm spins around a virtual center position to help counteract error from gradient estimation algorithm, **b** without spinning, **c** with spinning in mapping a contour
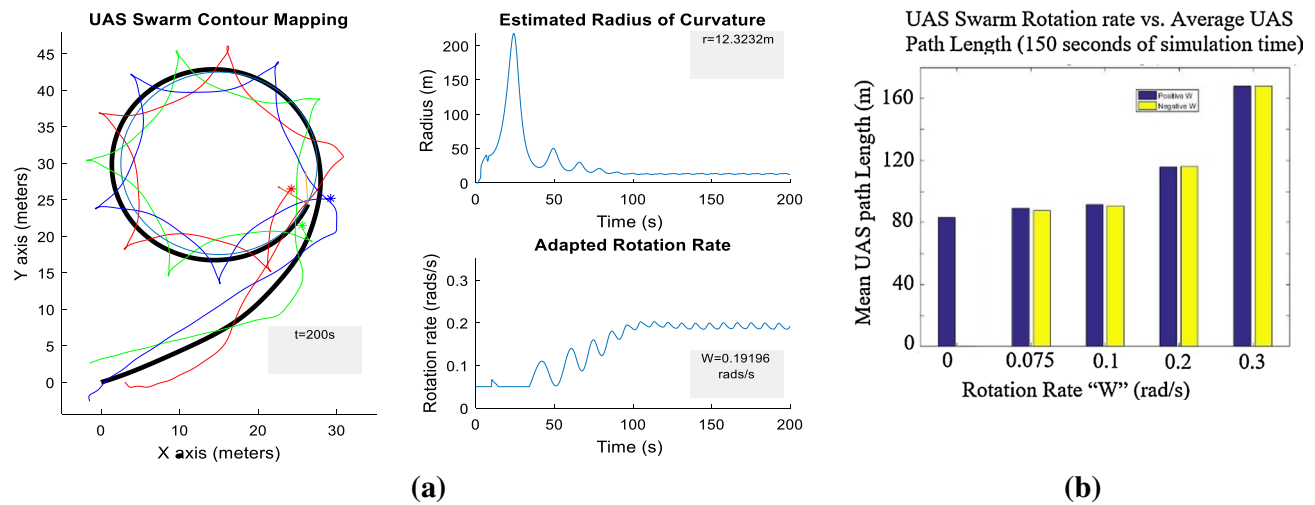
Fig. 9 **a** Adaptive tuning of spin rate based on the radius of curvature of a formation center path. In this example, as an estimated radius of curvature approaches the target contour located at 10 m, a spin rate

converges to desired 0.25 rad/s. **b** The plot of average path lengths in terms of different spin rates

0.05 rad/s and an upper bound of 0.3 rad/s. There is a big spike in a radius of curvature plot due to the nearly linear path the swarm has to follow. During the source-seeking stage, minimum spinning is maintained to save the total flight paths. Total path lengths in terms of spin rates are shown in Fig. 9b, which demonstrates a nearly negligible difference in path length if the swarm spins clockwise or counterclockwise. Rotation rates of $0, \pm 0.075, \pm 0.1, \pm 0.2$, and ± 0.3 rad/s are used to compare the average flight path lengths.

The simulation was also done for multiple peaks or radiation sources. Figure 10 shows the contour mapping simulation done for three radiative sources. As shown in Fig. 10, the proposed algorithm is capable of tracing the desired contour reasonably well.

The simulation was also done for a single moving radiation source. As shown in Fig. 11, the proposed algorithm can accomplish tracing of the desired radiation contour well if the source moves reasonably slow. Figure 11 shows a moving source traveling at 0.07 meters per second from (10, 40) m to (40, 10) m. Mapping this source is possible in this particular case because the speed of the swarm is traveling at roughly seven times the speed of the source.

4.2 UAS swarm simulation in an MCNP computed radiation field

The MCNP is a general purpose code applied to neutron, photon, and electron transport [21] for a realistic radiative field. A simulated radiative field with dimensions of 100 m
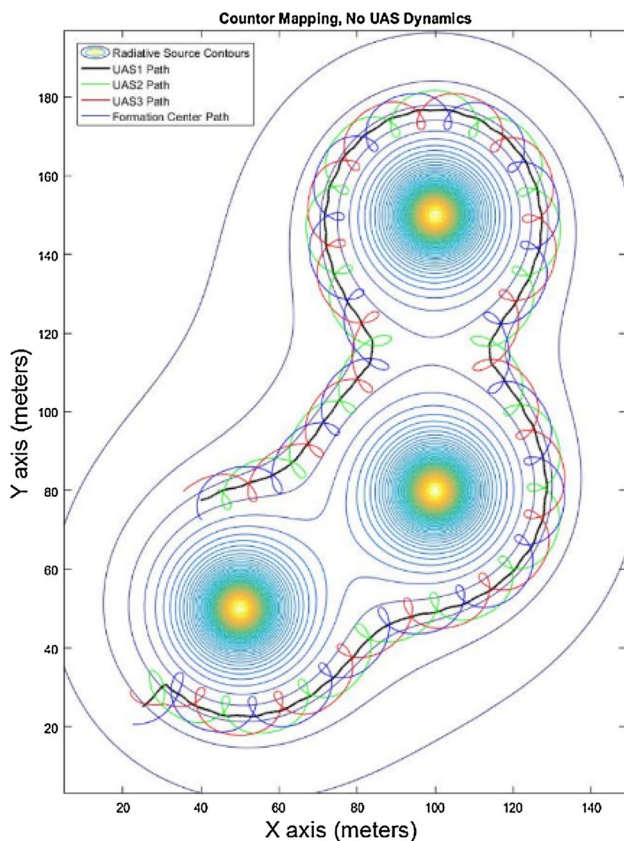
Fig. 10 Contour mapping is done for three radiation sources in the $1/R^2$ model

$\times$ 100 m $\times$ 32 m contains five sources of radiation ranging from 3 MeV to 6 MeV. As shown in Fig. 12, a concrete building is also introduced into the simulation to show what would happen if a building structure blocks certain areas of radiation detection by onboard sensors of UASs.

The desired reference contour is shown in Fig. 13 along with the actual performance of the contour mapping algorithm overlaid onto the radiative field. It should be noted that a two-dimensional radiation contour at the height of 15 m is used for this simulation. In this simulation, the swarm's starting position is located inside the radiation field at (35, 35). As shown in Fig. 13, the proposed algorithm successfully mapped the desired contour with reasonable accuracy.

5 Experiments

In this work, not a radiation source, but a light source simulating $1/R^2$ was used to validate key algorithms of contour mapping and source seeking in the indoor flight testbed. The testbed is outfitted with an OptiTrack motion capture system which allows real-time feedback of the position and orientation within the flight volume at 120 Hz. Two types of UAS

platforms are used. One platform, developed by Bitcraze, is the Crazyflie 2.0, an open-source quadcopter designed to be small, lightweight, and easily modifiable. The small size of the Crazyflie 2.0 allows for validation of the contour mapping algorithm with a virtual source. The other platform used for the experiment is the DJI Flamewheel 450, chosen for the experiment where an onboard light sensor can be used for source-seeking behavior validation. Figure 14a, b shows Crazyflie 2.0 and Flamewheel F450 with a single-board computer mounted under the frame. The robot operating system (ROS) is used in both platforms as an open-source tool. It works through the use of nodes and topics, and the nodes can either publish a topic, subscribe to a topic or both as shown in Fig. 14c.

5.1 Gradient estimation

In order to verify the algorithm of gradient estimation by three UASs in a circular formation, each UAS platform was placed upside down roughly equiangular around the center of the flight volume as shown in Fig. 15a. Each UAS was placed at 0.5 m radius away from the center. The light source, acting as a radiation source analog, is moved around in a circle concentric with the swarm. The data captured through a wireless sensor network are fed to the gradient estimation algorithm. Positions of a light source and three UASs are identified by the OptiTrack motion capture system and are used to compute the true values of the gradient based on the $1/R^2$ assumption. Figure 15b shows that the proposed gradient direction estimation scheme agrees with the measured ones reasonably well. It should be noted that the source distance of 0.7 m was used, which is rather too small for an actual contour mapping application. As expected, gradient direction estimation error reached almost 30° which are rather too big for accurate mapping operation. However, it should be noted that experimental measurement has a good agreement with computed ones as shown in Fig. 15b.

5.2 Source-seeking behavior

Due to space constraints for using the DJI Flamewheel F450 in our flight volume, the source-seeking experiment was carried out to test the gradient estimation algorithm for the heading angle rather than contour mapping. A light source is placed on a movable dolly within the flight volume and moved along the *x*-axis to show that gradient estimation is successful in determining the direction of the source using the data of the light sensors from each UAS. The swarm is restricted to move along the *x*-axis, and the reference position generation is bound to $\pm$ 0.5 m. This is chosen to minimize the risk of the swarm crashing into the sides of the flight volume. The tracking of the light source and three UAS platforms is
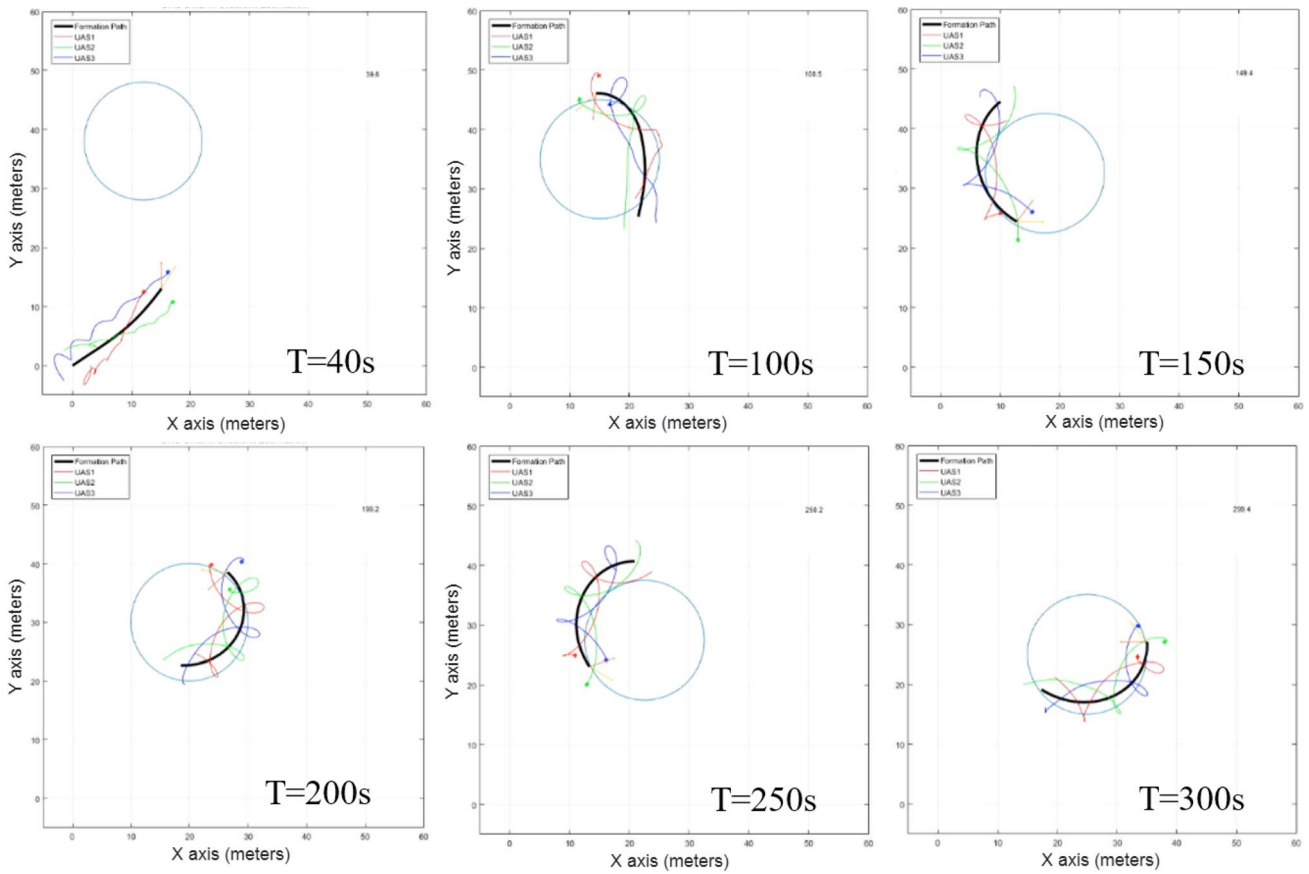
Fig. 11 Contour mapping is done for a single moving source in the $1/R^2$ model
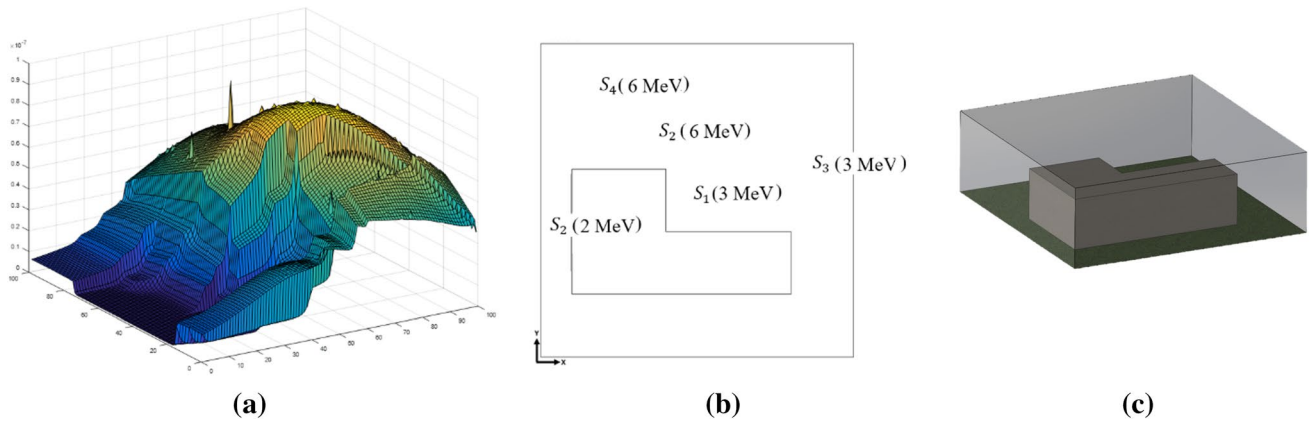

Fig. 12 Simulated radiation field (height of 15 m) with a concrete structure and multiple radiation sources using MCNP: **a** simulated radiative map. **b** Locations of five radiation sources. **c** A simulated field with the physical structure

done via the OptiTrack motion capture system. Note that Fig. 16a shows an embedded window to display source-seeking performance in real time using the motion capture system in the flight volume. Figure 16b shows how the UAS swarm center moves as the source is moved as the expected oscillatory motion of the swarm center occurs due to gradient estimation errors by a finite number of light sensors.
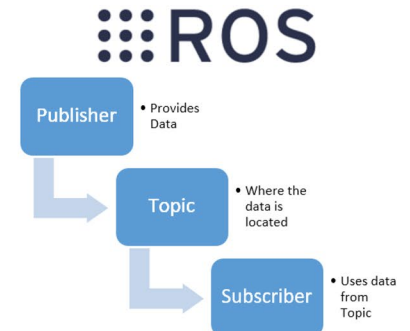
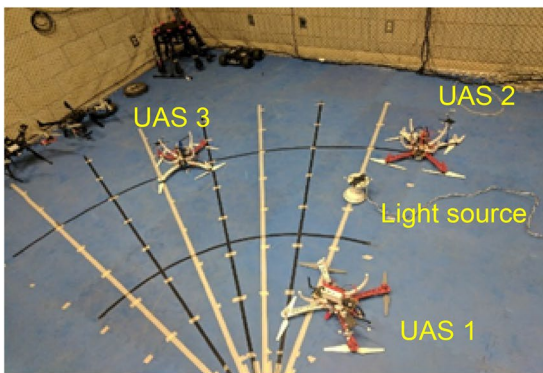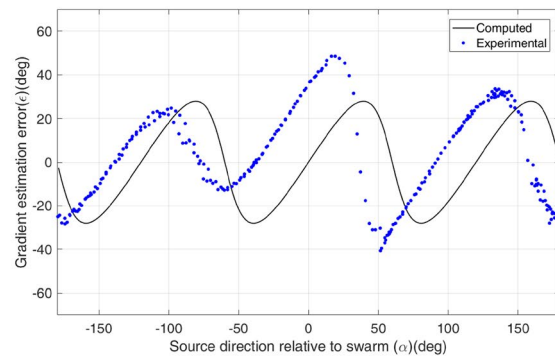**Fig. 13** Contour mapping simulated in the radiation field simulated using the MCNP code
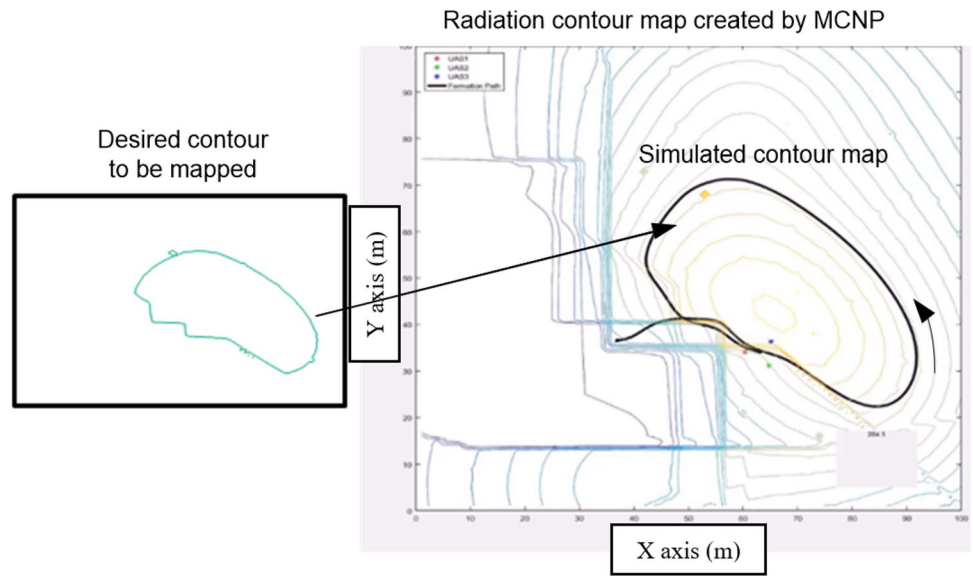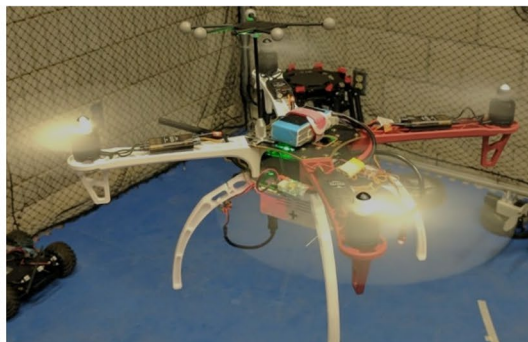
Fig. 14 Technical specifications of two platforms used for the experiment, **a** Crazyflie 2.0, **b** DJI Flamewheel 450, **c** control and communication using ROS

Fig. 15 **a** Experimental setup for gradient estimation scheme. **b** Plots of gradient estimation errors with respect to source direction
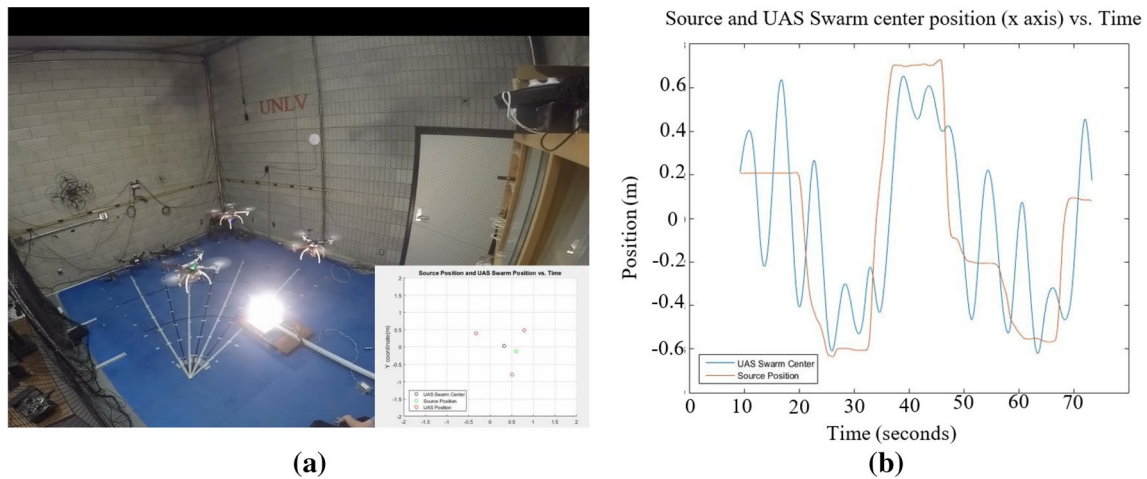
Fig. 16 **a** Source-seeking behavior experiment using a light source and three lux sensors. **b** The plot of source and swarm center positions

5.3 Contour mapping behavior

To demonstrate the effectiveness of the proposed contour mapping algorithm, three Crazyflies are used due to the limited size of the indoor flight volume. Also, a virtual source is used due to a limited payload and communication capability of the Crazyflie platform. As shown in Fig. 17a, a virtual source is located on the ground and the OptiTrack system tracks both the source and each swarm agent. The "source strength" needed for the gradient estimation algorithm is calculated using the $1/R^2$ model where R is obtained from the virtual source position data from each UAS. Figure 17b shows the plot of swarm center motion following the reference contour defined with respect to a virtual source located on the floor. The experimental results of the contour mapping are shown in Fig. 17b. It maps the reference contour by ± 0.1 m, which is less than 8% of the size of the contour.

6 Conclusions

This research developed the method of contour mapping and source seeking in the radiation field by UAS swarm equipped with radiation detectors. The method is especially suitable for low-altitude applications where fixed-wing UAS is not suitable for use. The source seeking and contour mapping algorithms are developed based on a simple $1/R^2$ radiation field, but they are validated for more realistic radiation field with scattering and attenuation effects simulated by MCNP code. It showed successful implementation of the proposed algorithm for mapping radiation contours for multiple and moving radiation sources. It also showed an effective way of cutting down flight trajectories of three flying platforms by adaptively updating a swarm spin rate based on averaging radiation
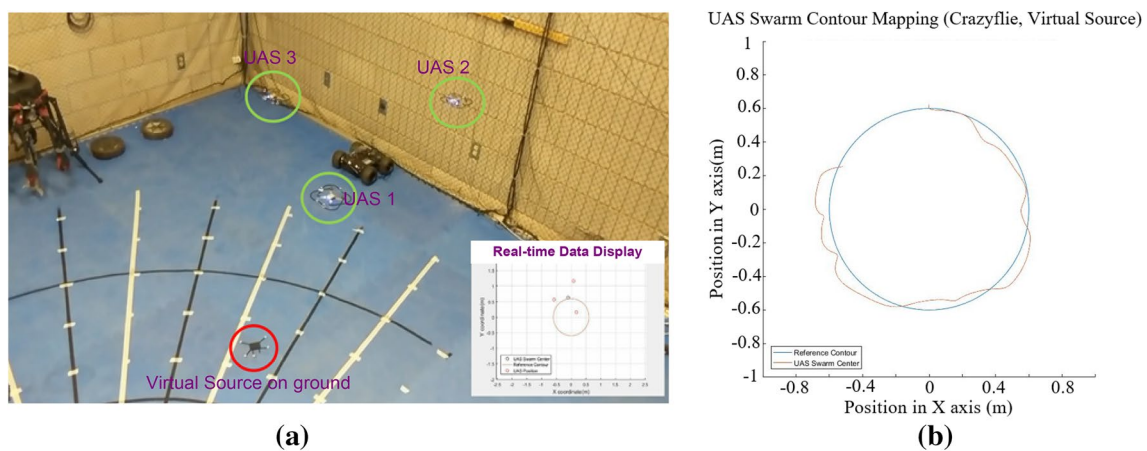

Fig. 17 **a** Contour mapping experiment with the swarm of three Crazyflie 2.0 UAS (circled in green) and a virtual source (circled in red) along with a real-time data display window. **b** Actual trajectory of the swarm's center (color figure online)

measurements. The proposed UAS swarm can survey an unknown environment and map the area to help first responders effectively manage operations and safeguard personnel while locating the radiation sources to enhance situational awareness.

References

1. Gilbertson M (2013) US Department of Energy (DOE), experience and strategic lessons learned from decommissioning and remediation of large nuclear legacy sites. In: International experts' meeting on decommissioning and remediation after a nuclear accident

2. Sen TK, Moore LJ (2000) An organizational decision support system for managing the DOE hazardous waste cleanup program. Decis Support Syst 29(1):89

3. Brewer ET (2009) Autonomous localization of $1/R^2$ sources using an aerial platform autonomous localization of $1/R^2$ sources using an aerial platform. M.S. Thesis, Virginia Polytechnic Institute and State University

4. Sepulchre R, Paley DA, Leonard NE (2007) Stabilization of planar collective motion: all-to-all communication. IEEE Trans Automat Control 52(5):811–824

5. Leonard NE, Paley DA, Lekien F, Sepulchre R, Fratantoni DM, Davis RE (2007) Collective motion, sensor networks, and ocean sampling collective motion, sensor networks, and ocean sampling. Proc IEEE 95(1):48–74

6. Raffard RL, Tomlin CJ, Boyd SP, Formulation AP (2004) Distributed optimization for cooperative agents: application to formation flight. IEEE Conf Decis Control 3:2453–2459

7. Marshall JA, Broucke ME, Francis BA (2004) Formations of vehicles in cyclic pursuit. IEEE Trans Automat Control 49(11):1963–1974

8. Ogren P, Egerstedt M, Hu X (2002) A control Lyapunov function approach to multiagent coordination. IEEE Trans Robot Autom 18(5):847–851

9. Arranz LB, Seuret A, De Wit CC (2009) Translation control of a fleet circular formation of AUVs under finite communication range. Proc IEEE Conf Decis Control 98:8345–8350

10. Moore BJ, Canudas-de-Wit C (2010) Source seeking via collaborative measurements by a circular formation of agents. In: American control conference (ACC)

11. Cortez RA, Tanner HG (2008) Radiation mapping using multiple robots. Trans Am Nucl Soc 99:157–159

12. Han J, Chen Y (2014) Multiple UAV formations for cooperative source seeking and contour mapping of a radiative signal field. J Intell Robot Syst 74(1–2):323–332

13. Cui R, Li Y, Yan W (2016) Mutual information-based multi-AUV path planning for scalar field sampling using multidimensional RRT. IEEE Trans Syst Man Cybernet Syst 46(7):993

14. Hitz G, Galceran E, Garneau M, Pomerleau F (2017) Adaptive continuous-space informative path planning for online environmental monitoring. J Field Robot 34:1427–1449

15. https://www.kromek.com/index.php/products/applications/radiation-detection/gr1-gamma-ray-spectrometer

16. https://www.kromek.com/index.php/products/nuclear-technology/czt/gr1a

17. Kazemeini M, Barzilov A, Yim W, Lee J (2018) Integration of CZT and CLYC radiation sensors into a UAS platform. In: Proceedings of conference on sensors and electronic instrumentation advances (SEIA'18), Amsterdam, Netherlands, pp 57–59. 19–21 Sept 2018

18. Kazemeini M, Cook Z, Lee J, Barzilov A, Yim W (2018) Plug-and-play radiation sensor components for unmanned aerial system platform. J Radioanal Nucl Chem 318:1797–1803

19. Ogren P, Fiorelli E, Leonard NE (2004) Cooperative control of mobile sensor networks: adaptive gradient climbing in a distributed environment. IEEE Trans Automat Control 49(8):1292–1302

20. Uryasev S (1995) Derivatives of probability functions and some applications. Ann Oper Res 56(1):287–311

21. Goorley T (2012) Initial MCNP6 release overview. Nucl Technol 180(3):298–315